As cast and heat-treated alloys of the Pt-Al-V system at the Pt-rich corner

by B.O. Odera*†‡, L.A. Cornish*†‡, M.B. Shongwe*‡, G.O. Rading†§ and M.J. Papo‡¶

Synopsis

The Pt-based alloys have a high potential for replacing some Ni-based superalloys (NBSAs) used in the highest temperature and most aggressive environments, and vanadium would be a beneficial alloying element.

Six alloys of average compositions Pt-26.6Al-9.1V, Pt-23.1Al-17.8V, Pt-9.6Al-21.1V, Pt-17.4Al-6.4V, Pt-22.3Al-7.9V, and Pt-6.0Al-10.1V (all in at.%) were manufactured by arc-melting and examined in the as-cast condition using scanning electron microscopy and X-ray diffraction (XRD). Five samples were heat treated at 1 000°C for 1 500 hours and water quenched, then examined. The phases were identified using energy-dispersive X-ray spectroscopy and the identities were confirmed by XRD. In most of the samples, the phases existing in the as-cast condition were different from those at 1 000°C after ~1500 hours heat treatment. A solidification projection, an isothermal section and a liquidus surface projection were determined for the Pt-rich corner.

Keywords
Phase diagram, Pt-Al-V system, scanning electron microscopy, X-ray diffraction.

Introduction

Nickel-based superalloys (NBSAs) have been successfully used in turbine components since the late 1940s. Approximately 70 percent of the weight of a modern jet turbine comprises NBSAs, and their success is due to their high yield stress and excellent resistance to environmental attack at high temperatures[1]. Although the NBSAs have excellent properties, they are hindered by their maximum application temperature, which is limited by the melting point of the nickel solid-solution matrix. Currently, the maximum temperature at which NBSAs operate is ~1 100°C, which is approximately 85 percent of their melting temperature[1]. If the operating temperatures could be increased, there would be a number of advantages. Higher temperatures improve the efficiency of the turbine engines, and this enables greater thrust, improved fuel efficiency, and reduced pollution. Although thermal-barrier coatings can be used to increase the application temperature, the component is still restricted by the melting point of the substrate, so the maximum attainable temperatures are still limited if catastropic failure is to be avoided[2].

There is increasing interest in using a different alloy system with a much higher melting point. Ceramics and selected intermetallic phases have been discussed because of their high melting points and high strength; however, both suffer from reduced toughness compared with NBSAs, and their processing costs are high[2]. One solution would be to base the new materials on alloys with high melting points and use the naturally occurring precipitates of that system. This should also help keep the processing cost to a minimum. Thus, the systems developed would be similar in structure to the NBSAs, with a matrix and a fine dispersion of small, preferably coherent and stable precipitates. Face–centered cubic (fcc) structures (like nickel) are advantageous because, being close-packed, they are more creep resistant. Refractory metals (niobium, molybdenum, and tungsten) have been considered because of their high melting points (2 469°C, 2 623°C, and 3 020°C respectively), but their more open body-centred cubic (bcc) structures are more susceptible to creep. Additionally, they are prone to rapid oxidation, even at relatively low temperatures[3]. Platinum-group metals (platinum, iridium, rhodium, and palladium) were targeted for investigation because, with the exception of palladium, they have high melting points, good environmental resistance, and a mostly fcc structure[4].

* *School of Chemical and Metallurgical Engineering, University of the Witwatersrand.*

† *African Materials Science and Engineering Network (AMSEN).*

† *DST/NRF Centre of Excellence in Strong Materials, hosted by University of the Witwatersrand.*

§ *Department of Mechanical and Manufacturing Engineering, University of Nairobi.*

¶ *Advanced Materials Division, Mintek.*

As cast and heat-treated alloys of the Pt-Al-V system at the Pt-rich corner

Pt is similar to Ni in crystal structure (fcc) and chemistry. The important differences are the higher melting point (1769°C for Pt compared to 1 455°C for Ni) and improved corrosion resistance[5]. These facts inspired Wolff's and Hill's research into the development of Pt-based analogues to Ni-based superalloys that could potentially serve in the most critical and demanding of the high-temperature applications[4]. Thus, phases similar to $L1_2$ Ni_3Al could be used to obtain properties similar to those found in the NBSAs. Although platinum-based alloys are unlikely to replace all NBSAs on account of both higher price and density, it is likely that they can be used for the highest application temperature components.

Alloys based on Pt-Al have the highest potential, not only because of possible precipitation strengthening through Pt_3Al, but also due to high oxidation and corrosion resistance. The resistance to oxidation and corrosion is attributed to the formation of a protective Al oxide scale[6,7]. At least 11 at.% Al is needed to form a thin protective oxide coating on the ternary and quartenary alloys at high temperatures[8]. It is generally accepted that the $L1_2$ structure of the γ' phase is a prerequisite for the success of the Ni-based superalloys. Due to the close crystallographic relationship, precipitates with ordered fcc, $L1_2$ have coherent interfaces with the surrounding fcc matrix. Coherent γ/γ' interfaces with small lattice misfit lead to low interfacial energies, thus prohibiting fast coarsening of γ'[8].

Under the auspices of the Platinum Development Initiative, platinum-based superalloys were investigated for high-temperature and special applications requiring good corrosion and oxidation resistance[9]. Ternary alloys based on Pt-Al, where the ternary additions comprised chromium, iridium, molybdenum, nickel, rhenium, ruthenium, tantalum, titanium, and tungsten were tested. As well as phase characterization work, mechanical and oxidation tests were undertaken. The best systems were found to be Pt-Al-Cr and Pt-Al-Ru. The microstructures were similar to NBSAs, and comprised ~Pt_3Al precipitates in a Pt-based matrix. However, the volume fraction of ~Pt_3Al was only ~40% instead of the ~70% found in the NBSAs[9].

Chromium was found to stabilize the cubic form of the ~Pt_3Al phase, whereas ruthenium acted as a solid-solution strengthener[10]. In order to exploit the additional benefits from the two ternary additions (Cr and Ru), quaternary alloys were made containing both. A number of these quaternary alloys have been investigated extensively. They exhibited a two-phase γ/γ' structures analogous to the NBSAs [11].

Much work has been done on the quarternary alloys of the Pt-Al-Cr-Ru system in an attempt to optimize the composition with respect to the precipitate volume fraction and hardness. The Vickers hardness of the Pt-Al-Cr-Ru alloys within the composition ranges selected was relatively independent of the chemical composition and the number of annealing stages and fell within the range HV_{10} ~400 to ~430. The volume fraction of the precipitate, using image analysis, was estimated at approximately 25 to 30%[12].

There is a need to increase the hardness and consequently the strength, melting temperature, and volume fraction of the precipitates. It is also desirable to reduce density and cost. Although vanadium may not meet all these requirements, it is expected to reduce cost and density by replacing some Pt in a chosen Pt-Al-Cr-Ru alloy. It is also expected to act as a solid solution strengthener by going into solution in (Pt), as well as increase the melting temperature. The binary phase diagram of Pt-V shows that ~20.5% V will go into solution in (Pt) at 700°C, increasing to ~57% at 1 720°C, and the melting temperature of (Pt) has a maximum of ~1 805°C[13]. Addition of Nb, Ta, and Ti to Pt-based alloys resulted in elevated strengths at high temperatures through precipitation-hardening. The polycrystalline Pt-based alloys containing 5 at.% Nb or Ta are stronger than the single-crystal NBSA CMSX-4 in (001) orientation above 1 200°C[14]. V is near Nb, Ta, and Ti in the periodic table and is smaller in size compared to Nb and Ta. Therefore, V may act as a precipitation-hardener in addition to solid-solution strengthening.

Experimental procedure

Six alloy buttons (Samples 1 to 6) weighing ~2 g each were prepared from Pt and Al of 99.9 percent purity and V of 99.6 percent purity. Each of the six alloys is named with respect to its average overall composition in at.% in the as-cast condition. The samples were manufactured by arc-melting under argon in a water-cooled copper hearth. Each button was turned over and re-melted three times to ensure thorough mixing of the elements.

Each of the samples was halved using a ceramic blade mounted in a Struers Secotom-10 cutting machine. The spindle speed was 3 500 r/min and a feed of 0.5 m/s was used. One half were prepared for metallographic examination, in the as-cast condition, by grinding on silicon carbide down to 1 200 grit, diamond polishing down to 1 μm and then final polishing by an oxide polishing system (OP-S).

Five of the other halves (samples 1H, 2H, 3H, 5H and 6H, where the number refers to the original as-cast sample and 'H' refers to the 1 000°C heat treatment) were placed in silica glass tubes 16 mm in diameter. The glass tubes were then made into vacuum ampoules by evacuating air and sealing while the vacuum pump was running. The ampoules with the samples were placed in a tube furnace and annealed at 1 000°C for 1 500 hours. Quenching was done by removing the glass ampoules from the furnace, dropping them in water and breaking the glass, as quickly as possible in order to retain the phases existing at 1 000°C. The samples were then prepared for metallographic examination in the same way as the as-cast samples.

The microstructures of all the alloys were analysed using a scanning electron microscope (SEM) model HR-NovaNano SEM200. Imaging in all the analyses was done using the backscattered electron (BSE) mode, while overall and phase compositions were determined by energy dispersive X-ray spectroscopy (EDX). Often it was difficult to discern between some of the phases, even in BSE mode because of the similarity in average atomic number of these phases. There was also the concern that orientation and different electron channelling would also change the contrast[15], therefore the morphology of the phases was also used to differentiate them. Since the interaction volume generating the X-rays can be as much as 3 μm across and deep (especially for higher atomic number elements), the analyses for smaller regions than this are an indication only. Usually, an accuracy of ±1 at.% would be expected for this technique. Spot analyses were used on single phases and areal analyses on two-phase regions. The compositions of each phase and overall

compositions were determined by taking EDX readings from at least five different areas and reporting the average and the standard deviation. X-ray diffraction (XRD) was used to confirm the phase identities.

Results

As-cast alloys

As-cast Alloy 1, average overall composition Pt-26.6Al-9.1V (at.%)

Figure 1 shows the microstructure of the as-cast Alloy 1. It consists of medium grey dendrites surrounded by a dark thin layer, light needles, and a eutectic comprising the light phase and a barely resolveable two-phase dark region. The compositions of these phases are shown in Table I. The medium grey dendrites were identified as ~Pt_3Al and the light needles as ~Pt_5Al_3. The thin dark layer on the dendrites was identified as ~Pt_3V. XRD confirmed the identities of these phases. Solidification started with the ~Pt_3Al dendrites, followed by peritectic formation of ~Pt_5Al_3 which then solidified independently as needles. The ~Pt_3Al dendrites and the ~Pt_5Al_3 needles reacted peritectoidally to form ~Pt_2Al. The next reaction was eutectic, forming β + ~Pt_5Al_3 and the β decomposed eutectoidally to form ~PtAl + ~Pt_5Al_3[13]. The final reaction was peritectoid formation of a thin layer of ~Pt_3V between the ~Pt_3Al dendrites and the ~Pt_5Al_3 needles.

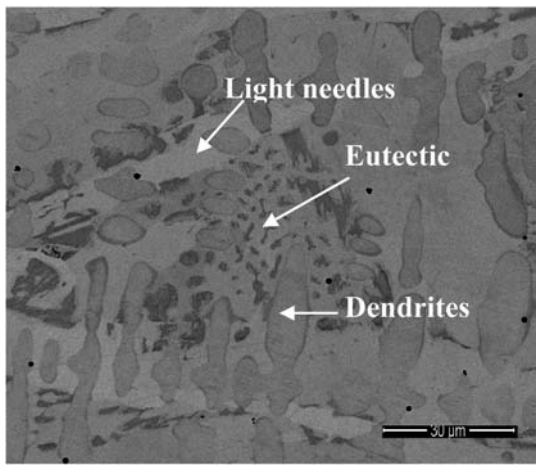

Figure 1—SEM-BSE image of Alloy Pt-26.6Al-9.1V (at.%) showing medium grey dendrites (~Pt_3Al) with a dark thin layer (~Pt_3V), light needles (~Pt_5Al_3), and a eutectic. Scale bar is 30 µm

As-cast Alloy 2, average overall composition Pt-23.1Al-17.8V (at.%)

Figure 2 shows the microstructure of the as-cast Alloy 2 at different magnifications. It consisted of medium grey dendrites surrounded by a light phase, also appearing dendritic, and a complex eutectic. When the compositions of these phases were plotted (Table II), the medium grey dendrites were identified as ~Pt_2V, the light phase as ~Pt_5Al_3, while the dark component of the eutectic was identified as PtAl, although the areas are likely to be affected by the nearby ~Pt_2V and ~Pt_5Al_3. XRD confirmed the identities of ~Pt_2V, ~Pt_5Al_3, and PtAl. Solidification started with (Pt). This was followed by a peritectic reaction between the (Pt) and the liquid, resulting in ~Pt_5Al. There then followed a eutectic reaction with the liquid forming ~Pt_5Al_3 and β, with β decomposing at high temperature to form PtAl + ~Pt_5Al_3[13]. The (Pt) dendrites ordered to ~Pt_2V (identified by unique peaks of those phases amongst the common peaks). There was also a solid-state cellular precipitation of ~Pt_2V /(Pt) in the ~Pt_5Al_3 phase, and these phases were too fine to analyse using SEM-EDX.

As-cast Alloy 3, average overall composition Pt-9.6Al-21.1V (at.%)

Figure 3 shows the microstructure of as-cast Alloy 3, average overall composition Pt-9.6Al-21.1V (at.%), at two different magnifications. It consists of dendrites, a light phase, and a dark phase between the dendrites. When the compositions of the phases in Table III were plotted, the dendrites were identified as ~Pt_3V, and the light phase as ~Pt_3Al. The dark phase was identified as ~Pt_2Al, which formed peritectoidally at high temperature from ~Pt_5Al_3 and ~Pt_3Al. Here, any ~Pt_5Al_3 that formed was consumed. Solidification started with (Pt), followed by a weak peritectic reaction between the liquid and (Pt) resulting in a sparse eutectic with the dark component ~Pt_2Al in the light ~Pt_3Al. The final reaction was (Pt) ordering to ~Pt_3V. XRD confirmed the phase identifications.

As-cast Alloy 4, average overall composition Pt-17.4Al-6.4V (at.%)

Figure 4 shows that the as-cast Alloy 4, average overall composition Pt-17.4Al-6.4V (at.%), consisted of a single phase having grains at different orientations. The gain was increased to enhance the contrast. The compositions in Table IV are for different grains i.e. orientations, and hence different contrast. The plot of these compositions confirmed

Table I

Overall and phase compositions of Alloy 1, average overall composition Pt-26.6Al-9.1V (at.%) as determined by EDX

Component	Pt	Al	V	Phases
Overall	64.3±0.7	26.6±0.8	9.1±0.4	-
Medium dendrites	67.4±0.6	18.7±0.6	14.0±0.5	~Pt_3Al
Dark	65.3±0.4	29.4±0.8	5.3±0.5	~Pt_2Al
Light needles	59.0±1.2	30.7±1.1	10.3±0.4	~Pt_5Al_3
Thin dark layer on dendrites	65.5±0.9	13.6±1.1	20.9±1.2	~Pt_3V
Eutectic overall	63.0±0.3	29.1±0.7	8.0±0.5	~PtAl + ~Pt_5Al_3

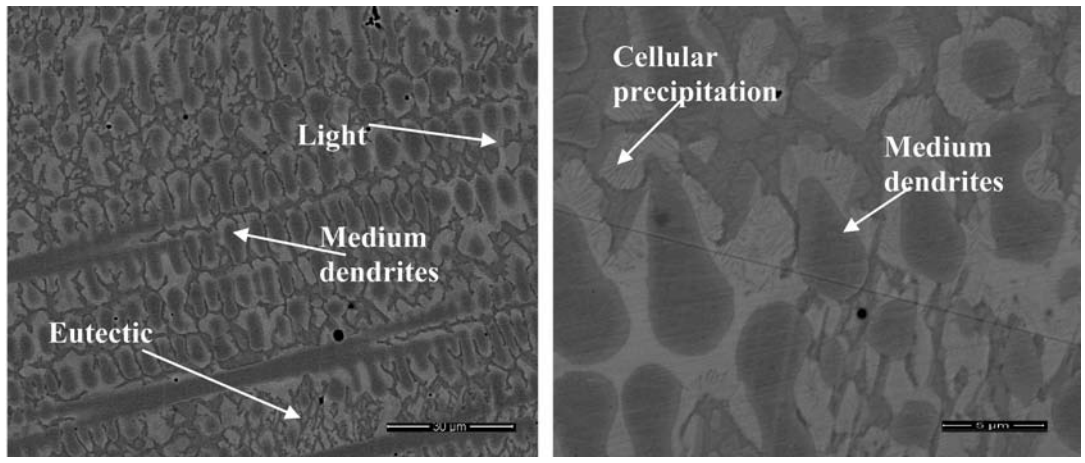

(a) (b)

Figure 2—(a) SEM-BSE image of Alloy 2 showing medium grey dendrites (~Pt2V), a light phase ~Pt_5Al_3), and a eutectic (β + ~Pt_5Al_3). Scale bar is 30 µm. (b) SEM-BSE image of Alloy 2 showing medium grey dendrites (~Pt_2V), a light phase (~Pt_5Al_3) and solid state cellular precipitation. Scale bar is 5 µm

Table II

Overall and phase compositions of Alloy 2, average overall composition $Pt_{59.1}$:$Al_{23.1}$:$V_{17.8}$ (at.%) as determined by EDX

Component	Pt	Al	V	Phases
Overall	59.1±0.3	23.1±0.4	17.8±0.1	-
Medium dendrites	60.5±0.4	8.3±0.4	31.2±0.4	~Pt_2V
Light phase	62.0±0.3	32.3±0.3	5.7±0.5	~Pt_5Al_3
Eutectic	58.2±0.4	25.7±1.2	16.1±1.0	~Pt_5Al_3 + β
Dark eutectic component (2-phase)	54.4±1.7	32.8±1.9	12.9±0.9	PtAl + ~Pt_5Al_3

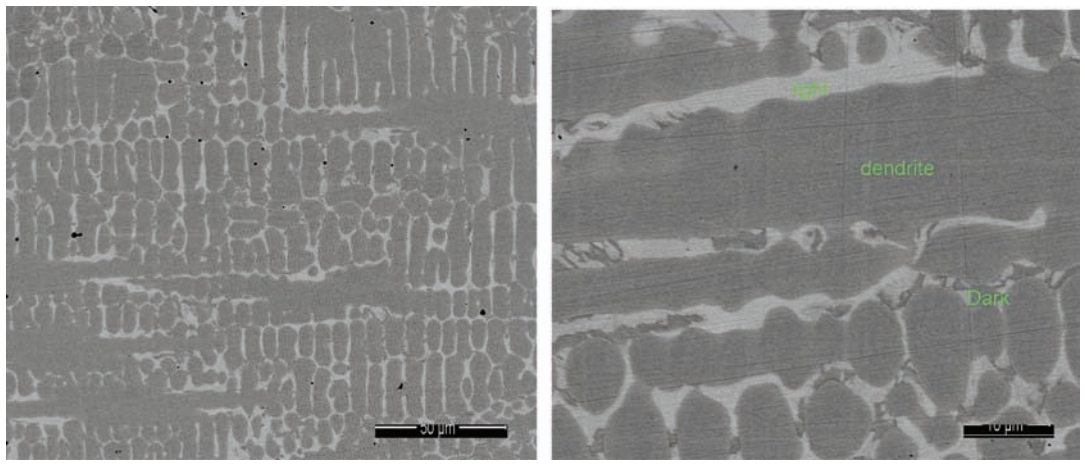

(a) (b)

Figure 3—(a) SEM-BSE image of as-cast Alloy Pt-9.6Al-21.1V (at.%) showing dendrites (~Pt_3V) and a light phase (~Pt_3Al). Scale bar is 50 µm. (b) SEM-BSE image of as-cast Alloy Pt-9.6Al-21.1V (at.%) dendrites (~Pt_3V), a light phase (~Pt_3Al) and a dark phase (~Pt_2Al) between the dendrites. Scale bar is 10 µm

Table III

Overall and phase compositions of Alloy 3, average overall composition Pt-9.6Al-21.1V (at.%) as determined by EDX

Component	Pt	Al	V	Phases
Overall	69.3±1.2	9.6±1.0	21.1±1.1	-
Dendrites	69.7±1.3	4.9±1.3	25.2±0.6	~Pt_3V
Light phase	69.8±0.4	25.5±0.6	4.7±0.6	~Pt_3Al
Dark	62.8±1.3	27.9±1.2	9.3±0.4	~Pt_2Al

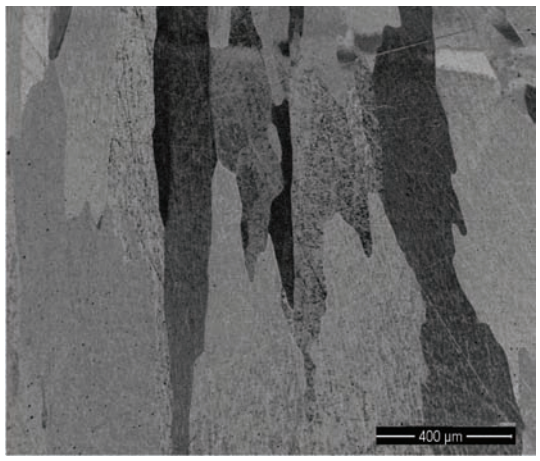

Figure 4—SEM-BSE image of as-cast Alloy $Pt_{76.2}Al_{17.4}V_{6.4}$ (at.%) showing a single phase (~Pt_3Al) with grains at different orientations. Scale bar is 400 µm

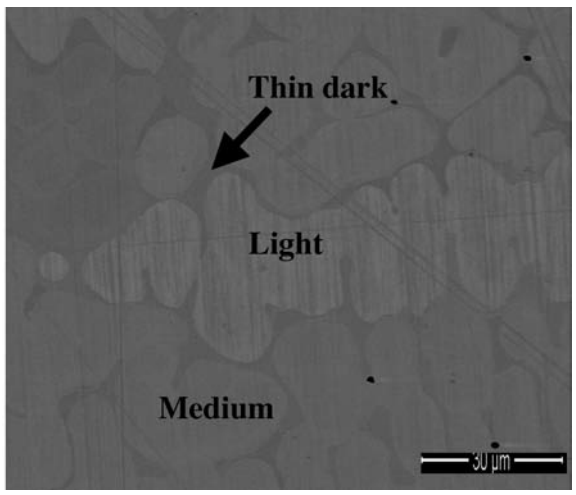

Figure 5—SEM-BSE image of as-cast Alloy Pt-22.3Al-7.9V showing a light grey phase (~Pt_3Al), a medium grey phase (~Pt_3Al) and a thin dark grey phase (~Pt_2Al). Scale bar is 30 µm

that the alloy was single phase ~Pt_3Al, and XRD also confirmed the phase identity.

As-cast Alloy 5, average overall composition Pt-22.3Al-7.9V (at.%)

Figure 5 is a SEM-BSE image of the microstructure of as-cast Alloy 5, showing light- and medium-contrast dendrites with a thin dark contrast phase. Since the average atomic numbers of the phases were similar, the contrast between them was low, giving a poor image. Both the light and medium grey phases were identified as ~Pt_3Al, from the close compositions and the same dendritic morphology, while the thin dark grey phase was identified as ~Pt_2Al from the composition. Solidification started with ~Pt_3Al, followed by a peritectic formation of a thin layer of ~Pt_5Al_3 which subsequently reacted peritectoidally with ~Pt_3Al, to form ~Pt_2Al.

As-cast Alloy 6, average overall composition Pt-6.0Al-10.1V (at.%)

Figure 6 shows the microstructure of as-cast Alloy 6, average overall composition Pt-6.0Al-10.1V (at.%), with a medium-contrast phase which was identified as (Pt) and a fine eutectic. The existence of the eutectic was confirmed after it coarsened during heat treatment for 1 500 hours at 1 000ºC (described later). The eutectic and its components were too fine to be analysed accurately by EDX. Solidification started with (Pt), followed by the eutectic reaction producing (Pt) and ~Pt_3Al. XRD confirmed the presence of (Pt) and ~Pt_3Al (Figure 7).

Table IV

Compositions of Alloy 4A, average overall composition Pt-17.4Al-6.4V (at.%) as determined by EDX

Component	Pt	Al	V	Phases
Overall	76.2	17.4	6.4	-
Dark	75.3±0.1	18.9±3.7	5.8±2.7	~Pt_3Al
Medium	76.4±0.3	16.6±1.0	7.0±0.9	~Pt_3Al
Light phase	75.7±0.1	17.6±1.5	6.8±1.6	~Pt_3Al

Table V

Compositions of Alloy 5, average overall composition Pt-22.3Al-7.9V (at.%) as determined by EDX

Component	Pt	Al	V	Phases
Overall	69.8±0.5	22.3±0.5	7.9±0.5	-
Light	70.6±0.3	21.2±0.1	8.2±0.2	~Pt_3Al
Medium	72.2±1.1	18.7±0.9	9.1±0.4	~Pt_3Al
Thin dark	65.8±0.2	30.4±0.2	3.8±0.3	~Pt_2Al

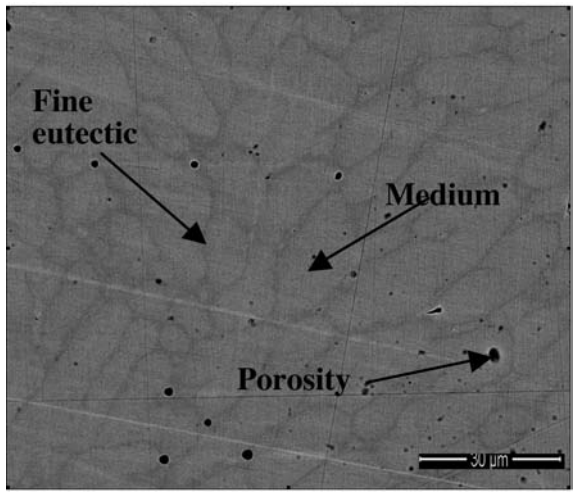

Figure 6—SEM-BSE image of as-cast $Pt_{83.9}$:Al_6:$V_{10.1}$ (at.%) showing a medium grey phase (Pt), a fine eutectic ((Pt) + ~Pt_3Al) and porosity (dark spots). Scale bar is 30 µm

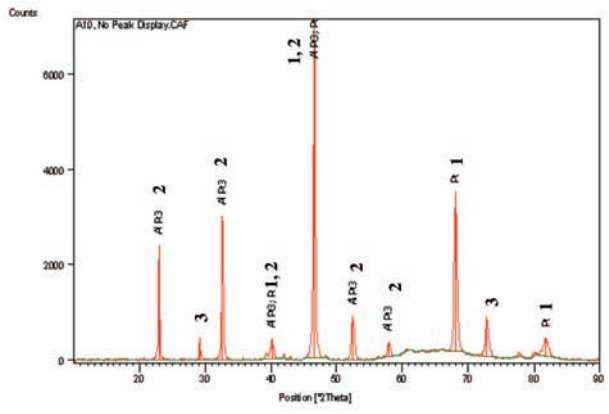

Figure 7—XRD pattern of as-cast Alloy 6, average overall composition Pt-6.0Al-10.1V (at.%). Key: (Pt) – 1, ~Pt_3Al – 2, and $CaCO_3$ - 3 in the resin mounting

Heat-treated alloys

Annealed Alloy 1H, average overall composition Pt-26.2Al-9.1V (at.%)

Figure 8 depicts the microstructure of annealed Alloy 1H, average overall composition Pt-26.2Al-9.1V (at.%), showing a medium-contrast phase, a light phase, a dark phase and a eutectic. In some cases, the medium contrast phase had a thin dark layer around it, indicating that these were the dendrites in the as-cast alloy although their composition had changed.

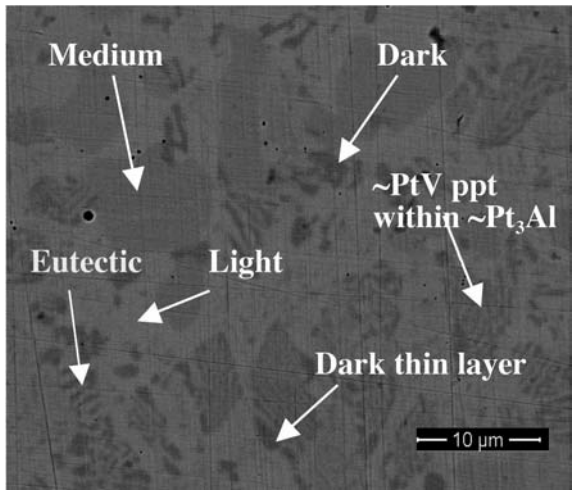

Figure 8—SEM-BSE image of annealed alloy $Pt_{64.7}$:$Al_{26.2}$:$V_{9.1}$ (at.%) showing a medium grey phase, a light phase, a dark phase, a eutectic, and dark precipitate the within medium grey phase. Scale bar is 10 µm

The original dendrites showed precipitates of a darker phase, presumed to be PtV considering the contrast and the morphology, which varied between coarse (easily visible) and fine (very difficult to resolve). The plot of the compositions identified the light phase as ~Pt_5Al_3, the dark phase as either ~PtV or ~Pt_2V, while the medium grey phase was identified as ~Pt_3Al. The individual components of the eutectic were too small to be analysed accurately by EDX. XRD confirmed the identity of the light phase as ~Pt_5Al_3 and the dark phase as ~PtV (Figure 9).

Annealed Alloy 2H, average overall composition Pt-21.1Al-17.1V (at.%)

Figure 10 shows images of annealed alloy 2H, average overall composition Pt-21.1Al-17.1V (at.%), at different magnifications. Figure 10(b) shows a dark phase with light solid-state precipitates and a light phase with dark solid-state precipitates. Plotting identified the dark phase as ~PtV and the light phase as ~Pt_5Al_3. The precipitates were too small to be analysed accurately by EDX. XRD confirmed the presence of ~PtV and ~Pt_5Al_3. Compared to the as-cast sample, the ~PtV dendrites had reduced in volume with precipitation of ~Pt_5Al_3, and the light matrix had aligned precipitates of ~PtV.

Annealed Alloy 3H, average overall composition Pt-10.8Al-25.5V (at.%)

Figure 11 shows Alloy 3H, average overall composition Pt-10.8Al-25.5V (at.%), at different magnifications. Figure

Table VI

Compositions of as-cast Alloy 6, average overall composition Pt-6.0Al-10.1V (at.%) as determined by EDX

Component	Pt	Al	V	Phases
Overall	83.9±0.3	6.0±0.3	10.1±0.3	-
Medium	88.5±0.4	3.2±0.51	8.3±0.3	(Pt)
Eutectic	78.1±7.2	12.1±2.1	9.8±5.6	(Pt) + Pt_3Al

As cast and heat-treated alloys of the Pt-Al-V system at the Pt-rich corner

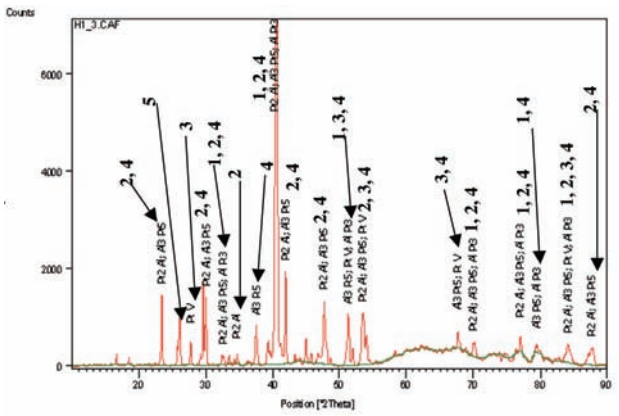

Figure 9—XRD pattern of Alloy 1H, average overall composition Pt-26.2Al-9.1V (at.%). Key: ~Pt_3Al - 1, ~Pt_2Al – 2, ~PtV – 3, ~Pt_5Al_3 – 4, $CaCO_3$ - 5

11(a) shows a medium grey phase, a light phase, and a dark phase. Comparison with the as-cast structure (Figure 3) shows that the amount of ~Pt_2V dendrites had been reduced, and a lighter phase, ~Pt_3Al, had precipitated within the dendrites (Figure 11 (b)). The phase was too small to analyse accurately, although larger areas of the medium phase were analysed. Plotting identified the medium phase as ~Pt_2V, the dark phase as ~PtV, while the light phase was identified as ~Pt_3Al. XRD confirmed these identities.

Annealed Alloy 5H, average overall composition Pt-23.2Al-7.1V (at.%)

Alloy 5H, average overall composition Pt-23.2Al-7.1V (at.%), contained a dark and a medium contrast phase of the same morphology and a small amount of a light phase. EDX compositions of the phases showed that the dark and

Table VII

Overall and phase compositions of annealed Alloy 1H, average overall composition Pt-26.2Al-9.1V (at.%) as determined by EDX

Component	Pt	Al	V	Phases
Overall	64.7±0.3	26.2±0.2	9.1±0.2	-
Medium dendrites	65.3±0.4	17.5±0.8	17.2±0.7	~Pt_3Al
Light phase	65.4±0.9	30.5±1.5	4.1±0.8	~ Pt_5Al_3
Dark phase	57.9±1.0	5.3±2.0	36.6±2.5	~PtV
Eutectic	63.8±1.2	24.5±2.5	11.8±1.5	?
Two-phase dendrites	66.0±0.5	20.4±1.1	13.6±1.3	~PtV pptn. within ~Pt_3Al

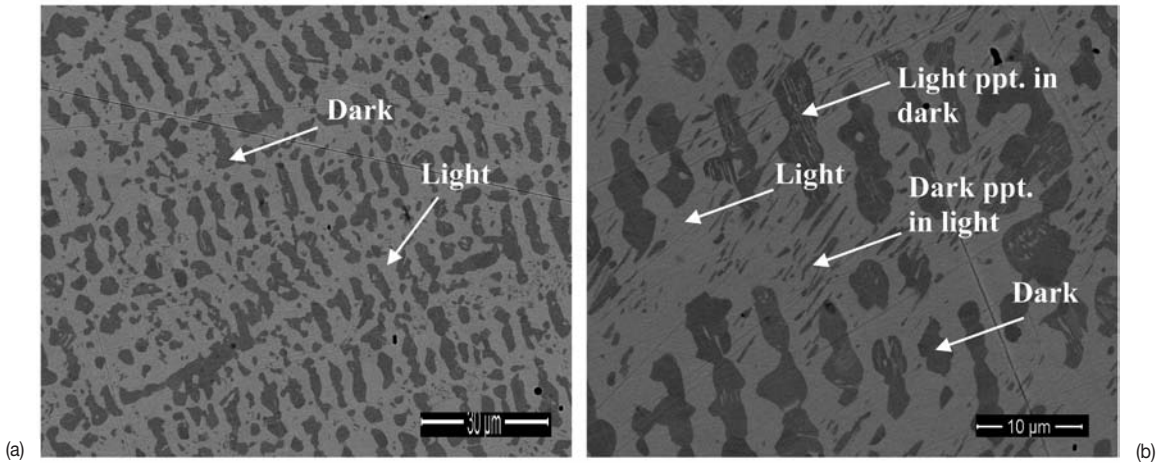

(a) (b)

Figure 10—(a) SEM-BSE image of annealed Alloy Pt-21.1Al-17.1V (at.%) showing a dark phase (~PtV), a light phase (~Pt_2Al) and dark precipitates in the light phase. Scale bar is 30 µm. (b) SEM-BSE image of annealed Alloy Pt-21.1Al-17.1V (at.%) showing a dark phase, a light phase, a eutectic, and a possible light precipitates in the dark phase. Scale bar is 10 µm

Table VIII

Overall and phase compositions of annealed Alloy 2H, average overall composition Pt-21.1Al-17.1V (at.%) as determined by EDX

Component	Pt	Al	V	Phases
Overall	61.8±0.3	21.1±0.6	17.1±0.3	-
Dark	57.6±0.4	1.8±0.2	40.6±0.2	~PtV
Light	64.4±0.3	33.8±0.4	1.8±0.2	~Pt_5Al_3
Dark ppt. within the light matrix	63.8±0.9	28.2±2.0	7.9±1.2	~PtV pptn. within ~Pt_2Al
Light ppt. within the dark phase	59.1±0.9	8.9±0.9	32.4±1.6	~Pt_5Al_3 pptn. within ~PtV

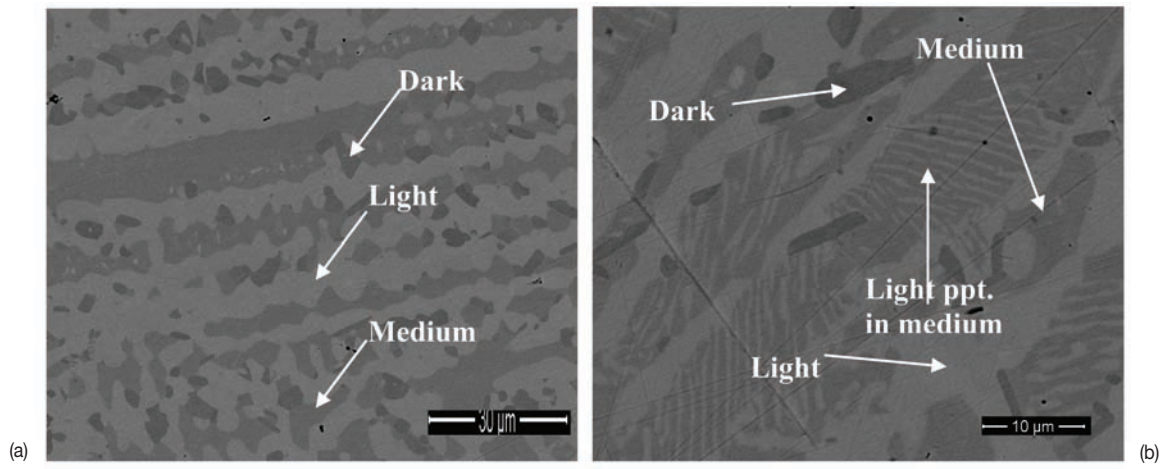

(a) (b)

Figure 11—(a) SEM-BSE image of annealed alloy Pt-10.8Al-25.5V (at.%) showing a medium grey phase (~Pt_2V), a light phase (~Pt_3Al), and a dark phase (~PtV). Scale bar is 30 µm. (b) Figure 11(b). SEM-BSE image of annealed alloy Pt-10.8Al-25.5V (at.%) showing a medium grey phase (~Pt_2V), a light phase (~Pt_3Al), a dark phase (~PtV), and 2-phase dendrites. Scale bar is 10 µm

Table IX

Overall and phase compositions of annealed Alloy 3H, average overall composition Pt-10.8Al-25.5V (at.%) as determined by EDX

Component	Pt	Al	V	Phases
Overall	63.7±0.5	10.8±0.6	25.5±0.3	-
Medium	64.0±0.4	3.2±0.5	32.8±0.6	~Pt_2V
Light	65.3±0.8	15.9±1.4	18.8±0.9	~Pt_3Al
Dark	58.4±0.6	0	41.5±0.6	~PtV
2-phase dendrites	64.2±0.6	7.4±0.7	28.3±0.3	~Pt_3Al pptn. within ~Pt_2V

Table X

Overall and phase compositions of annealed Alloy 5H, average overall composition Pt-23.2Al-7.1V (at.%) as determined by EDX

Component	Pt	Al	V	Phases
Overall	69.7±0.1	23.2±0.3	7.1±0.1	-
Dark	70.6±0.3	21.0±0.2	8.4±0.2	~Pt_3Al
Medium	70.4±0.6	21.6±1.0	8.1±0.7	~Pt_3Al
Light	65.0±0.7	32.7±0.7	2.2±0.2	~Pt_2Al

medium contrast phases were the same phase, ~Pt_3Al, and the appearance was likely due to different orientations. The light phase was identified as ~Pt_2Al. XRD confirmed the presence of both phases (Figure11).

Annealed Alloy 6H, average overall composition Pt-5.8Al-10.3V (at.%)

Figure 13 shows annealed Alloy 6H, average overall composition, Pt-5.8Al-10.3V (at.%), at different magnifications. Both have poor contrast owing to the close average atomic numbers of the phases. Figure 13(a) shows a light contrast phase and a dark phase. From the plotting, the light phase was identified as (Pt), and the dark phase as ~ Pt_2V, which was not observed in the as-cast sample. The coarsened eutectic could just be discerned in Figure 13(a) and was more

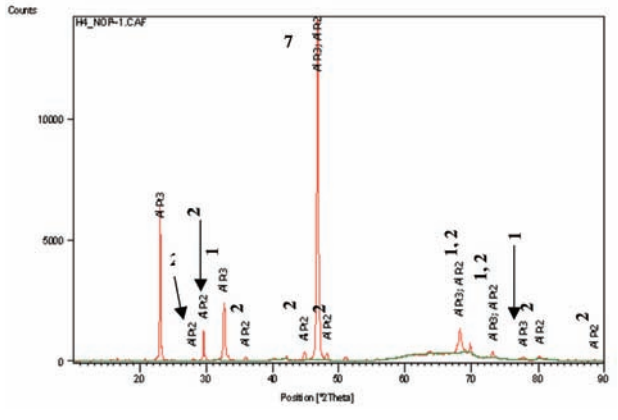

Figure 12—XRD pattern of alloy 5H, average overall composition Pt-23.2Al-7.1V (at.%). Key: ~Pt_3Al – 1 and ~Pt_2Al – 2

(a)

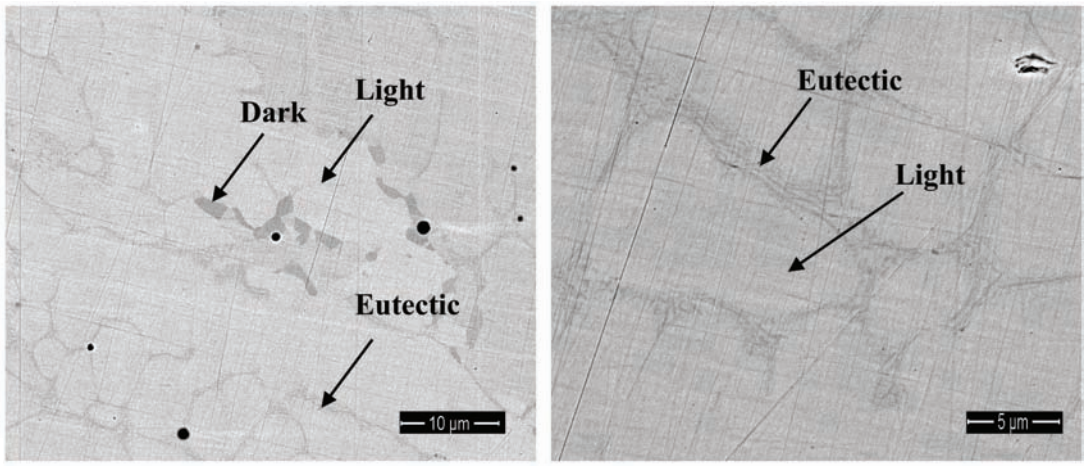

(b)

Figure 13—(a) SEM-BSE image of annealed alloy Pt-5.8Al-10.3V (at.%) showing a light grey phase (Pt), a dark phase (~Pt_2V), and a eutectic. Scale bar is 10 µm. (b) SEM-BSE image of annealed alloy Pt-5.8Al-10.3V (at.%) showing a light grey phase, and a eutectic at a higher magnification (x 10 000). Scale bar is 5 µm

Table XI

Overall and phase compositions of annealed Alloy 6H, average overall composition Pt-5.8Al-10.3V (at.%) as determined by EDX

Component	Pt	Al	V	Phases
Overall	83.9±0.9	5.8±0.6	10.3±0.5	-
Light	87.8±0.5	3.7±0.3	8.6±0.5	(Pt)
Dark	70.1±0.7	-	29.9±0.7	~Pt_2V
Eutectic	78.5±1.0	6.8±0.2	14.8±1.2	(Pt) + ~Pt_3Al

clearly resolved in Figure 13 (b). The components of the eutectic were too small to be analysed accurately by EDX. Extrapolation indicated that the eutectic is between (Pt) and ~Pt_3Al. XRD confirmed the presence of ~Pt_2V, ~Pt_3Al, and (Pt).

Discussion

Although some of the phases were very difficult to resolve, mainly because they had very similar average atomic numbers, the morphologies, analyses, and XRD results were consistent, even if the alloys were not fully homogeneous.

The solidification projection, obtained from the as-cast samples, at the Pt-rich corner is given in Figure 14, although changes to the phase field boundaries are expected as more alloys are studied. All the phases identified in the as-cast alloys were extensions of the binary phases. The phase ~Pt_3Al extended the most, particularly in the annealed condition (Figure 15).

The (Pt) phase had a greater solubility for Al above ~20 at.% V than between 10–20 at.% V. The annealed results were used to obtain the isothermal section in Figure 15. There were similar shapes for the phase field boundaries in the solidification projection and the isothermal section, particularly for (Pt) between 10–20 at.% V. It is not yet possible to discern the shape of the ~Pt_3Al phase field boundary on the Pt-rich side, but new samples are in preparation.

Alloy 1 had four visible phases, ~Pt_3Al, ~Pt_2Al, ~Pt_5Al_3, and ~Pt_3V, in the as-cast condition, while a fifth phase, PtAl, could not be resolved. In the annealed condition Alloy 1 contained ~PtV, ~Pt_5Al_3 and ~Pt_3Al. The light phase was deduced to be to be ~Pt_5Al_3 on the basis of not showing the

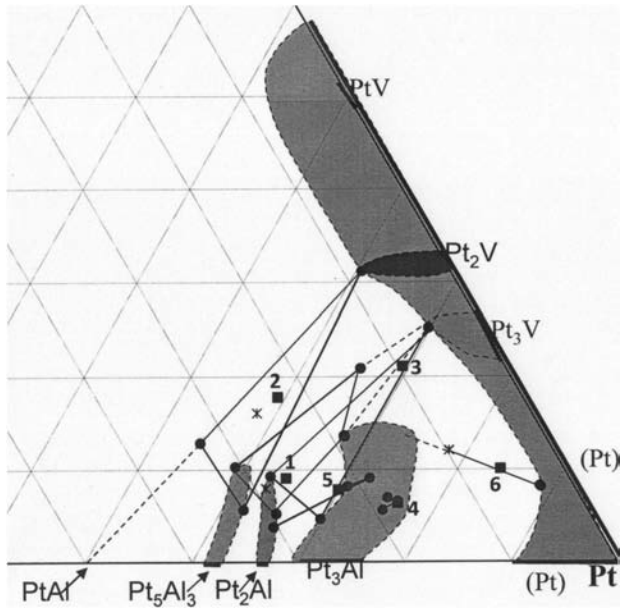

Figure 14—Solidification projection of the Pt-Al-V system at the Pt-rich corner

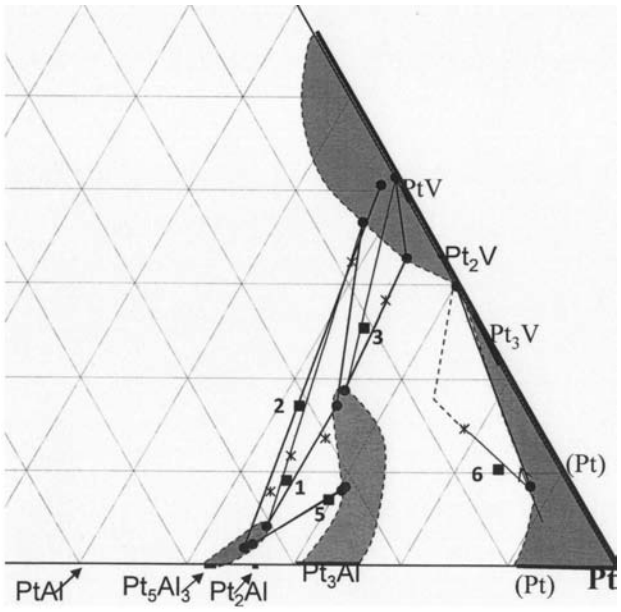

Figure 15—Isothermal section at 1 000°C of the Pt-Al-V system at the Pt-rich corner

laths as found by Tshawe *et al.*[16] in the Pt-Al alloys as well as the XRD pattern. The major change is that in the as-cast condition the alloy contained ~Pt_3V, while in the annealed condition it contained ~PtV. The change can be attributed to diffusion as the phase compositions change, or a reaction in which ~Pt_3V changed to ~PtV (although the involvement of the other phases cannot be identified yet). The microstructure of the annealed alloy was also coarser than that of the as-cast, which is expected.

Alloy 2 contained three phases in the as-cast condition, namely ~Pt_2V, ~Pt_5Al_3, and PtAl. There was a lamellar structure which consisted of a solid-state cellular precipitation of ~Pt_2V /(Pt) in ~Pt_2Al, which shows that the ~Pt_5Al_5 solvus retreats at lower temperatures. The complex eutectic was originally ~Pt_5Al_3 + β, and the β decomposed eutectoidally[13] to give almost unresolveable ~Pt_5Al_3 + ~PtAl. The annealed Alloy 2H contained two phases, ~PtV, ~Pt_5Al_3, and the remnants of a eutectic. The precipitation of ~PtV within the ~Pt_2Al matrix (Figure 9 (b)) shows that the ~Pt_5Al_3 solvus range decreases markedly with lower temperatures, as seen by the cellular precipitation in the as-cast alloy (Figure 2 (b)). Additionally, there was precipitation of ~Pt_5Al_3 within the ~PtV dendrites, which shows that the ~PtV solvus retreats substantially with decreasing temperature.

Alloy 3 contained three phases, ~Pt_3V, ~Pt_3Al, and ~Pt_2Al (in a small proportion), in the as-cast condition. In the annealed condition, there was ~Pt_2V, ~PtV, and ~Pt_3Al, and precipitation of ~Pt_3Al in the ~Pt_2V phase.

Alloy 4, which had an average overall composition Pt-17.4Al-6.4V, was single-phase ~Pt_3Al in the as-cast condition. This alloy has not yet been heat treated. Alloy 5 had an average overall composition Pt-22.3Al-7.9V, with two phases, ~Pt_3Al and ~Pt_2Al in the as-cast condition and the same two phases after annealing.

Alloy 6 contained (Pt) dendrites and a (Pt) + ~Pt_3Al eutectic in the as-cast condition. After annealing, the alloy had the same (Pt) and the (Pt) + ~Pt_3Al eutectic as well as a third phase, ~Pt_2V which must have formed as a result of a reaction during annealing.

Conclusion

The solidification projection, an isothermal section, and a liquidus surface projection for the Pt-rich corner of the Pt-Al-V were found to be consistent with each other. Using the solidification sequences from the phases and their morphologies, a tentative liquidus surface was derived. The ~Pt_2Al phase forms only in the solid state, and so does not appear on the liquidus surface.

Figure 16 (b) shows the solidification reactions for each of the as-cast alloys. These are schematic, since the analysed primary phase is assumed not to change on further solidification. Solidification starts with the composition moving directly away from the primary solid (on that primary

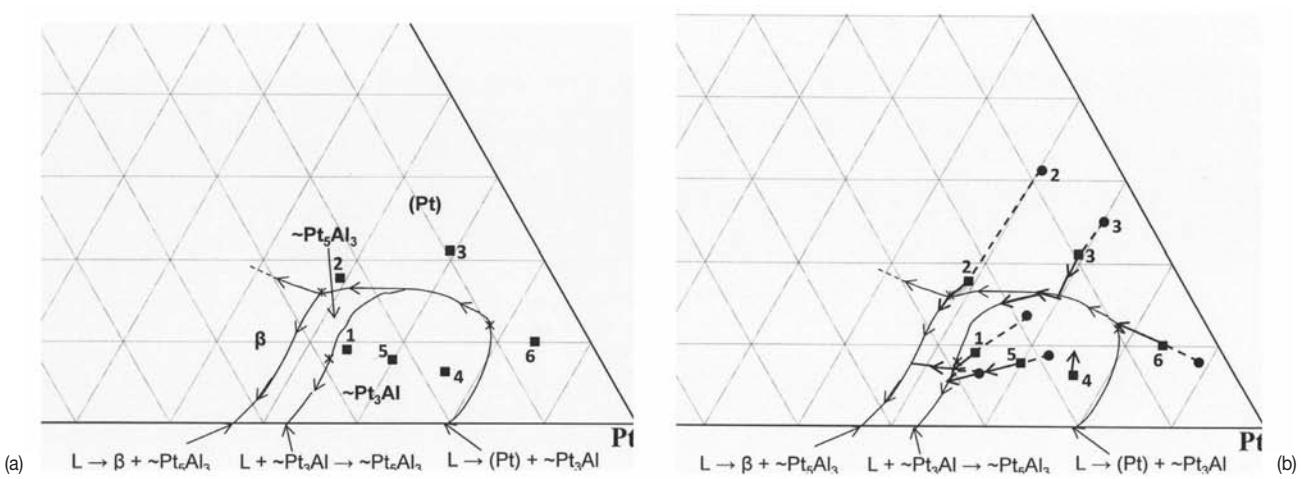

Figure 16—(a) Liqiudus surface projection for Pt-Al-V at the Pt-rich corner. (b) Solidification reaction on the liquidus surface for Pt-Al-V at the Pt-rich corner

liquidus surface) until a boundary with another liquidus surface is met, and the liquid composition then follows the boundary between the two liquidus surfaces for either a eutectic or a peritectic reaction (ignoring the fact that on non-equilibrium cooling, the liquid composition can sometimes run across the liquidus surface of the peritectic component. For Alloy 1, the second phase was also used to derive the direction of the liquid composition as the ~Pt_5Al_3 formed peritectically. Unfortunately the extrapolation of this falls on the direction of the liquidus for Alloy 5, but this is of no significance and is coincidental. Of the reactions observed, all had been reported in the Pt-Al binary, except for the peritectoid reaction ~Pt_3Al + ~Pt_5Al_3 → ~Pt_3V, which formed as a thin layer.

Several phases showed solid state-precipitation, indicating that the solvus of the original phase retreats noticeably with decreasing temperature. These included ~Pt_3Al, ~Pt_5Al_3, ~Pt_2V, and ~PtV. The solidification projection and the isothermal section were consistent with each other.

Acknowledgements

The authors would like to thank AMSEN, the DST/NRF Centre of Excellence in Strong Materials, National Research Foundation and Department of Science and Technology, Mintek, Dr. Elma van der Lingen, Mr. Mokae Bambo, Mr. Richard Couperthwaite, and Mr. Edson Muhuma for their support and assistance at various stages in the project.

References

1. Sims, C.T., Stoloff, N.S., and Hagel, W.C. Superalloys II: High Temperature Materials for Aerospace and Industrial Power. Wiley-Interscience, New York, NY, 1987. pp. 27–57.
2. Cornish, L.A., Fischer, B., and Völkl, R. Development of platinum-group-metals superalloys for high temperature use. *MRS Bulletin*, vol. 28, no. 9, September 2003. pp. 632–638.
3. Briant, C.L. High-Temperature Silicides and Refractory Alloys. Briant, C.L., Petrovic, J.J., Belaway, B.P., Vasudevan, A.K., and Lipsitt, H.A. (eds). *Mat. Res. Soc. Symp. Proc.* vol. 322, Pittsburg, 1994. pp. 305.
4. Wolff, I.M. and Hill, P.J. Platinum metals-based intermetallics for high temperature service. *Platinum Metals Review*, vol. 44, no. 4, 2000. pp. 158–166.
5. Süss, R., Cornish, L.A., Hill, P.J., Hohls, J., and Compton, D.N. Properties of a new series of superalloys based on $Pt_{80}Al_{14}Cr_3Ru_3$. *Proceedings of a Symposium on Advanced Materials and Processes for Gas Turrbines held in Copper Mountain, Colorado, USA*. G.E. Fuchs, G.E., James, A.W., Gabb, T., Maclean, M., and Harada, H. (eds). Sep. 22–26 2002. pp. 301–307.
6. Felten E.J. and Petit, F.S. Development, growth and adhesion of Al_2O_3 on platinum-aluminium alloys. *Oxidation of Metals*, vol. 10, no. 3, 1976, pp. 189–223.
7. Hill, P.J., Ellis, P., Cornish, L.A., Witcomb, M.J., and Wolff, I.M. The oxidation behaviour of Pt-Al- alloys at temperatures between 1 473 and 1 623 K. *Proceedings International Symposium on High Temperature Corrosion and Protection*, 2000. pp. 185–190.
8. Süss, R., Hill, P.J., Ellis, P., and Wolff, I.M. The oxidation resistance of Pt-based γ/γ' analogues to Ni-based superalloys. *Proceedings of the 7th European Conference on Advanced Materials and Processes*, Rimini, Italy, 2001.
9. Cornish, L.A., Süss, R., Douglas, A., Chown, L.H., and Glaner, L. The Platinum Development Initiative: Platinum-based alloys for high temperature and special applications: Part 1. *Platinum Metals Review*, vol. 53, no. 1, 2009. pp. 2–10.
10. Hill, P.J., Adams, N., Biggs, T., Ellis, P., Hohls, J., Taylor, S.S., and Wolff, I.M. Platinum alloys based on Pt-Pt_3Al fpr ultra-high temperature use. *Materials Science Engineering*, vol. A 329–331, 2002. pp. 295–304.
11. Cornish, L.A., Hohls, J., Hill, P.J., Prins, S., Süss, R., and Compton, D.N. J. The development of platinum-based alloys and their thermodynamic database. *Mining and Metallurgy,* vol. 38, no. 3–4, 2002. pp. 197–204.
12. Shongwe, M.B., Odera, B., Samal, S., Ukpong, A.M., Watson, A., Süss, R., Chown, L.H., Rading, G.O., and Cornish, L.A. Assessment of Microstructures in the development of Pt-based alloys. *Light Metals Conference,* Southern Africa Institute of Mining and Metallurgy, Johannesburg, 2010. p. 184.
13. Massalski, T.B. Binary Alloy Phase Diagrams. vol. 1, 2nd ed., ASM International, Materials Park, OH,1990. pp. 195-197.
14. Wenderoth, M., Voberg, S., Fischer, B., Yamabe-Mitarai, Y., Harada, H., Glatzel, U., and VölKl, R. Influence of Nb, Ta, and Ti on microstructure and high temperature strength of precipitation hardened Pt-base alloys. *Materials Science and Engineering*, vol. A 483–484, 2008. pp. 509–511.
15. Cornish, L.A., Witcomb, M.J., Coetzee, S., Tshawe, W., and Prins, S. Anomalies and pitfalls in phase analysis using BSE. *Proceedings of Microscopy Society of Southern Africa Conference*, vol. 38, 2008. pp. 9.
16. Tshawe, W., Douglas, A., Joja, B., and Cornish, L.A. A study of the Pt_3Al, Pt_2Al and β phases in the Pt-Al system. *Proceedings of Microscopy Society of Southern Africa Conference*, vol. 36, 2006. p. 15. ◆